universe

MDPI

Article

The Impact of Recent LUNA Measurements of NeNa Reactions on ^{26}Al Stellar Nucleosynthesis

Umberto Battino [1,2*,†] on behalf of The NuGrid Collaboration, Tommaso Gallo [3], Diego Vescovi [2,4], Sergio Cristallo [2,4], Andreas Best [1,5], Oscar Straniero [2,6], Eliana Masha [7], Erin R. Higgins [8,9] and Raphael Hirschi [10,†]

1 Department of Physics, University of Naples Federico II, Via Cintia, 80126 Napoli, Italy
2 Istituto Nazionale di Astrofisica (INAF)–Osservatorio Astronomico d'Abruzzo, Via M. Maggini, 64100 Teramo, Italy
3 Department of Physics, University of Oxford, Parks Rd., Oxford OX1 3PU, UK
4 Istituto Nazionale di Fisica Nucleare (INFN)-Sezione di Perugia, Via A. Pascoli, 06123 Perugia, Italy
5 Istituto Nazionale di Fisica Nucleare (INFN)-Sezione di Napoli, Via Cintia, 80126 Napoli, Italy
6 INFN-Sezione di Roma, pz. Aldo Moro 2, 00185 Roma, Italy
7 Helmholtz-Zentrum Dresden-Rossendorf, Bautzner Landstraße 400, 01328 Dresden, Germany
8 Armagh Observatory and Planetarium, College Hill, Armagh BT61 9DG, UK
9 Astrophysics Research Centre, School of Mathematics and Physics, Queen's University Belfast, Belfast BT7 1NN, UK
10 Astrophysics Group, Keele University, Keele, Newcastle-under-Lyme ST5 5BG, UK
* Correspondence: umberto.battino@inaf.it
† The NuGrid Collaboration: http://nugrid.github.io.

Abstract

Recent measurements performed by the LUNA(Laboratory for Underground Nuclear Astrophysics) collaboration between 2019 and 2024 have provided the most precise direct determinations to date of several key reaction rates in the NeNa cycle, specifically the ^{20}Ne$(p,\gamma)^{21}$Na and the ^{22}Ne$(p,\gamma)^{23}$Na reactions, as well as its bridge to the MgAl cycle, i.e., the ^{23}Na$(p,\gamma)^{24}$Mg reaction. Despite their improved accuracy, these updated rates are not yet consistently incorporated into widely used nuclear reaction network compilations. We explore the astrophysical impact of adopting the new LUNA rates by performing nucleosynthesis calculations, focusing on the case of ^{26}Al nucleosynthesis and considering four different stellar environments: low-mass AGB stars, massive stars, very massive stars and core-collapse supernovae. Our results show substantial sensitivity of ^{26}Al production to the revised rates. In the AGB model, the surface ^{26}Al abundance decreases by up to 30%, while in the massive star model, the ^{26}Al abundance in the C-burning shell increases by 51%. In contrast, the impact on both the ^{26}Al yields ejected by very massive stars and on the explosive nucleosynthesis in the supernova model is negligible. These findings have direct implications for galactic chemical evolution, the global budget of ^{26}Al, and theoretical predictions of the ^{60}Fe/^{26}Al ratio, which will be critically tested by forthcoming γ-ray observations from missions such as the Compton Spectrometer and Imager (COSI).

Keywords: evolved stars; stellar evolution; stellar interiors; nucleosynthesis

Academic Editor: Fridolin Weber

Received: 16 December 2025
Revised: 18 February 2026
Accepted: 25 February 2026
Published: 2 March 2026

1. Introduction

The synthesis of intermediate-mass nuclei in stellar interiors is governed by a network of proton capture reactions belonging to the CNO, NeNa, and MgAl cycles. These reactions play essential roles in setting the nucleosynthetic output of a wide variety of astrophysical

environments, such as hydrostatic hydrogen burning in both low-mass and massive stars, hot-bottom burning in asymptotic giant branch (AGB) stars, and explosive hydrogen burning in nova events. Accurate thermonuclear reaction rates for these processes are therefore crucial for reliable stellar models, galactic chemical evolution studies, and predictions of key observational tracers, such as the galactic distribution of radioactive ^{26}Al (with a half-life of 0.72 Myr).

Between 2019 and 2024, the LUNA (Laboratory for Underground Nuclear Astrophysics) collaboration carried out a program of deep-underground measurements targeting many key NeNa and MgAl reactions. Conducted at the underground accelerator facility of the INFN Gran Sasso Laboratory, the LUNA experiments benefit from the exceptionally low cosmic-ray background resulting from ~1400 m of rock overburden, enabling direct measurements at energies close to the Gamow windows of quiescent stellar burning. This environment is particularly favorable for reactions with extremely small cross sections, where surface laboratories are hindered by cosmic-ray-induced backgrounds. The objective of the LUNA campaign was to reduce longstanding nuclear physics uncertainties in the NeNa and MgAl cycles. This was achieved by providing precise, direct measurements suitable for modern stellar modeling for the ^{20}Ne$(p,\gamma)^{21}$Na, the ^{22}Ne$(p,\gamma)^{23}$Na and the ^{23}Na$(p,\gamma)^{24}$Mg nuclear reaction.

The first one of these reactions to be remeasured was the ^{23}Na$(p,\gamma)^{24}$Mg reaction, a key link between the NeNa and MgAl cycles [1]. Changes in this reaction rate can shift abundances between sodium and magnesium isotopes, indirectly influencing the subsequent production of ^{26}Al. The LUNA experiments described by [1] provided the first accurate, direct measurement of the low-energy resonances that dominate the rate in stellar interiors, dramatically tightening the uncertainty budget associated with the MgAl cycle and reducing rate uncertainties from factors of several to typically tens of percent.

Later on, the LUNA collaboration also published a revised measurement of the ^{20}Ne$(p,\gamma)^{21}$Na reaction, which represents the entry point into the NeNa cycle [2]. Precise knowledge of this rate is essential for modeling hydrogen burning in both massive stars and explosive environments, where it controls the conversion of ^{20}Ne into heavier species. The updated LUNA result resolves longstanding uncertainties in the low-energy cross section and provides the most accurate rate currently available.

Completing the series, the ^{22}Ne$(p,\gamma)^{23}$Na reaction regulates the flow between the Ne and Na isotopes in the NeNa cycle and controls the production of ^{23}Na in stars. Previous compilations relied on extrapolations or indirect measurements, resulting in uncertainties of up to an order of magnitude at astrophysical energies. The LUNA measurement program was designed explicitly to address this issue by performing a series of deep-underground studies, identifying low-energy resonances, and improving the astrophysical S-factor [3]. The resulting reaction rate is the most precise determination available to date, significantly reducing the uncertainty in the ^{22}Ne+p channel over the temperature range relevant to nucleosynthesis in both AGB stars and massive stars.

Collectively, the LUNA measurements of ^{20}Ne+p, ^{22}Ne+p, and ^{23}Na+p represent the most precise experimental determinations of these reactions published to date. Despite this, they are not yet consistently included in widely used reaction rate compilations for many stellar evolution and nucleosynthesis codes. This mismatch between the state of the art in nuclear experiments and the rates commonly adopted in astrophysical modeling motivates a reassessment of the impact of the new measurements on stellar nucleosynthesis calculations. One nucleus of particular interest is the radioactive isotope ^{26}Al, whose galactic γ-ray emission at 1.809 MeV has been observed for several decades and serves as a powerful tracer of ongoing nucleosynthesis. Multiple astrophysical sites contribute to the galactic inventory of ^{26}Al, including massive stars, core-collapse supernovae, AGB

stars, and possibly novae (e.g., [4]). The balance between production and destruction channels for ^{26}Al depends sensitively on the reaction flows through both the NeNa and MgAl cycles. In particular, the ^{23}Na$(p,\gamma)^{24}$Mg rate influences the availability of ^{25}Mg and ^{26}Mg, key progenitors of ^{26}Al [5], while the ^{22}Ne(p,γ) reaction governs the upstream abundance patterns that seed the entire process. Changes in these rates can therefore propagate into significant variations in predicted ^{26}Al yields. Moreover, the importance of accurate ^{26}Al predictions extends beyond stellar modeling. Galactic chemical evolution calculations rely on robust stellar yields to reproduce the observed mass of $\sim$3 M$_\odot$ of ^{26}Al in the Milky Way inferred from γ-ray surveys [6]. Furthermore, the ratio of ^{60}Fe/^{26}Al provides a sensitive diagnostic of massive star nucleosynthesis and will be probed with unprecedented precision by upcoming missions such as the Compton Spectrometer and Imager (COSI, [7]).

In this work, we systematically assess the impact of adopting the new LUNA rates in modern stellar models by computing nucleosynthesis predictions for four distinct stellar nucleosynthesis sites: namely low-mass AGB stars, hydrostatic burning in massive stars (M $\geq$ 10 M$_\odot$) and very massive stars (hereafter VMS, M $\geq$ 100 M$_\odot$), and core-collapse supernovae. For each case, we quantify the impact of replacing the default JINA REACLIB rates with the updated LUNA measurements of the ^{20}Ne$(p,\gamma)^{21}$Na, ^{22}Ne$(p,\gamma)^{23}$Na, and ^{23}Na$(p,\gamma)^{24}$Mg reactions, focusing in particular on changes to ^{26}Al production. In Section 2, we describe the numerical framework adopted for the stellar evolution and post-processing nucleosynthesis calculations; Section 3 presents the resulting nucleosynthetic abundances for the AGB star, massive star, and core-collapse supernova models. Finally, we summarize our main conclusions in Section 4.

2. Computational Methods

2.1. Simulation Setup

We considered a massive (15 M$_\odot$, Z = 0.006) stellar structure model computed with the stellar code MESA (revision 3709; [8]) and two low-mass AGB ones (2 M$_\odot$, Z = 0.0001 and Z = 0.001) computed with the FuNS code [9,10]. The low metallicities in the low-mass AGB cases were selected due to the more efficient production of NeNa isotopes compared with cases of higher metallicity [11]. The complete nucleosynthesis was computed using large nuclear network calculations.

The nucleosynthesis resulting from the massive star and VMS model was obtained using a post-processing code and the pre-calculated stellar structures detailed in [12]. The post-processing code mppnp is described in detail in [13]. The stellar structure evolution data were used as the input and processed with mppnp, meaning that the full nucleosynthesis was computed separately, thereby requiring less computing time and resources. In summary, at each stellar evolution time step, the 1097-isotope nuclear reaction network (extending up to Bi) is solved using a first-order Newton–Raphson backward Euler integration, followed by an implicit diffusion solver. The network adapts its problem size at each time step, and for each computational grid cell, based on the reaction flux of each isotope at the current state.

To ensure consistency between the stellar evolution and nucleosynthesis calculations, we verified that the rates of nuclear reactions relevant to energy generation, and thus to the evolution of the star, used in the MESA model were consistent with those adopted in mppnp for the full nucleosynthesis computation. The nuclear reaction rates adopted are the same as in [12], with the exceptions of the ^{22}Ne$(\alpha$,n$)^{25}$Mg and ^{22}Ne$(\alpha,\gamma)^{26}$Mg reaction rates, for which we use [14], and neutron captures on Ge and Se isotopes, for which we use [15–18].

The explosive nucleosynthesis case was computed using an explosive single-zone trajectory extracted from the explosion of the massive star model just introduced, at mass coordinate M = 2.66 M$_\odot$, in the CO shell, where the largest production of ^{26}Al is obtained.

The explosion simulation is discussed in [12], and this trajectory is the same as that presented in [19]. The local temperature and density peaks during the CCSN explosion are 2.39 GK and 1.18×10^5 g cm^{-3}.

In the case of the low-mass AGB models, a comprehensive nuclear network involving about 500 isotopes, from ^{1}H to ^{209}Bi, connected by more than 800 reactions, is coupled with the standard one-dimensional hydrostatic differential equations that describe the stellar structure. Magnetic-buoyancy-induced mixing has been included to model the formation of the ^{13}C pocket [20]. This additional mixing leads to an *s*-process nucleosynthesis pattern that differs significantly from that predicted by models relying on single-exponential convective overshoot to form the ^{13}C reservoir, and shows better agreement with available observational constraints [20–23]. The adopted baseline input physics is described in detail in [24]. In this work, we employ an updated isotopic composition based on [25], combined with the elemental abundances of C, N, O, and Ne from [26]. The main neutron source, the ^{13}C(α,n)^{16}O reaction, follows the rate provided by [27]. For the ^{22}Ne(α,n)^{25}Mg and ^{22}Ne(α,γ)^{26}Mg reactions, we adopt the rates from [14], consistent with the choices made for the massive star case.

2.2. Description of the Stellar Models

To evaluate the impact of the new LUNA reaction rates on ^{26}Al, we calculated the nucleosynthesis of the models presented in Section 2.1, adopting two different reaction rate selections for the ^{20}Ne(p,γ)^{21}Na, ^{22}Ne(p,γ)^{23}Na, and ^{23}Na(p,γ)^{24}Mg nuclear reactions, as summarized in Table 1. The nuclear reaction rates adopted in the `JINA` case correspond to the default reaction rate library in the JINA-REACLIB database [28]; in particular, the ^{20}Ne(p,γ)^{21}Na rate is from [29], the ^{22}Ne(p,γ)^{23}Na rate is from [30], and the ^{23}Na(p,γ)^{24}Mg rate is from [31]. In the `LUNA` case, the ^{20}Ne(p,γ)^{21}Na rate is from [2], the ^{22}Ne(p,γ)^{23}Na rate is from [3], and the ^{23}Na(p,γ)^{24}Mg rate is from [1]. We did not include the ^{25}Mg(p,γ)^{26}Al reaction, i.e., the main production channel of ^{26}Al because its `LUNA` measurement, detailed in [32], is already incorporated into the current `JINA` REACLIB default library.

Table 1. Schematic view of the references adopted for the two reaction rate selections presented in this work.

Nuclear Reaction	`JINA`	LUNA
^{20}Ne(p,γ)^{21}Na	Lyons et al., 2018 [29]	Masha et al., 2023 [2]
^{22}Ne(p,γ)^{23}Na	Kelly et al., 2017 [30]	Takacs et al., 2024 [3]
^{23}Na(p,γ)^{24}Mg	Iliadis et al., 2010 [31]	Boeltzig et al., 2019 [1]

In our VMS and AGB models, ^{26}Al is synthesized in the H-burning shell beneath the convective envelope at temperatures between 0.05 and 0.07 GK, while in our massive star model, it is produced mainly at temperatures between 1 GK and 1.4 GK during the hydrostatic shell C-burning phase, and at around 2.39 GK during the supernova explosion. Figure 1 shows the rate ratio of the rates listed in Table 1 between their `JINA` and `LUNA` values. Apart from temperature values lower than $\sim 3 \times 10^7$ K, which correspond to nuclear reaction timescales that are too long to affect the astrophysical scenarios considered in the present work, it is clearly visible that the ^{20}Ne(p,γ)^{21}Na and ^{22}Ne(p,γ)^{23}Na reaction rates from the `LUNA` both display a minimum in their ratio to the corresponding `JINA` values at temperatures typical of shell C-burning in massive stars, being approximately 15% and 20% below unity, respectively. Regarding the ^{23}Na(p,γ)^{24}Mg `LUNA` rate, we note that its ratio to the `JINA` rate reaches a minimum instead at H-burning shell temperatures in AGB stars.

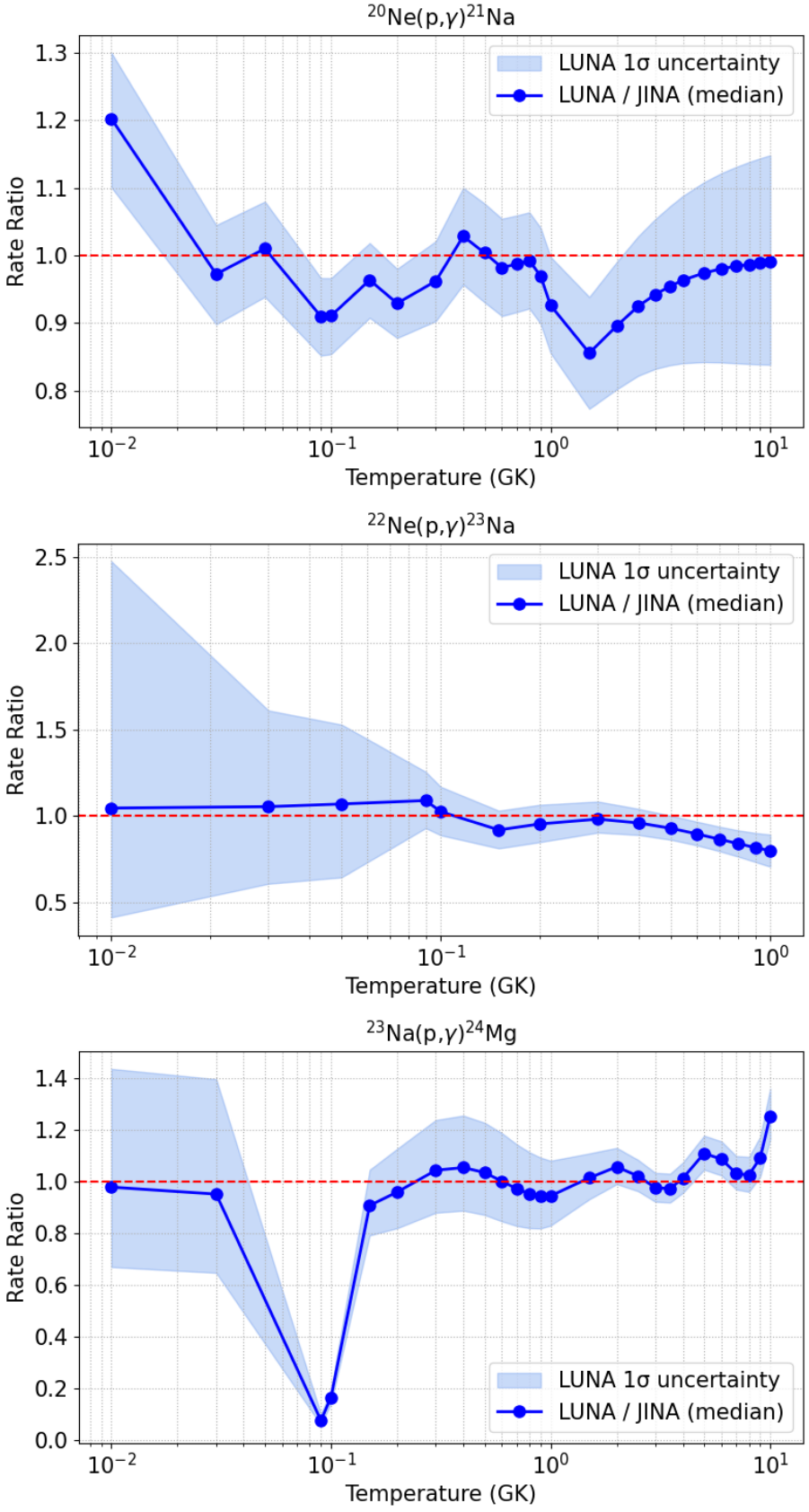

Figure 1. (**Upper panel**): Comparison of the LUNA and JINA ^{20}Ne(p,γ)^{21}Na nuclear reaction rate ratio as a function of temperature. The uncertainty band at the 1σ level is also included for the LUNA rates. (**Middle panel**): same as in the upper panel, but for the ^{22}Ne(p,γ)^{23}Na reaction. (**Lower panel**): same as in the upper panel, but for the ^{23}Na(p,γ)^{24}Mg reaction.

3. Impact of New Nuclear Reaction Rates on Stellar Nucleosynthesis

In this section, we present the complete nucleosynthesis computations of our stellar models using the two network settings detailed in Table 1.

3.1. Low-Mass AGB Models

Despite not being the main source of ^{26}Al in the Galaxy, AGB stars may still contribute to the enrichment of the interstellar medium in ^{26}Al. According to current estimates, about 0.1 $M_{\odot}$ of ^{26}Al has been ejected by AGB stars into the interstellar medium over the last million years [33]. During the interpulse period in the H-burning shell (located just below the extended H-rich convective envelope), ^{26}Al is efficiently produced through proton capture on abundant ^{25}Mg. The ^{25}Mg itself is mainly synthesized via the ^{22}Ne(α,n)^{25}Mg reaction in the He-intershell, situated between the H-burning shell and the electron-degenerate CO core, during recurring He-flashes. Each He-flash drives the expansion and cooling of the envelope and extinguishes the H-burning shell. As a result, plasma opacity and the radiative temperature gradient increase, while the entropy barrier at the formerly active H-burning shell decreases. This reduction allows convective motions to penetrate into the He-intershell, dredging the *s*-process, He-burning, and H-burning products (including ^{26}Al) up to the stellar surface [34–36].

The resulting surface abundance ratios in our low-mass AGB models for the `LUNA` case relative to the `JINA` case for stable isotopes of Ne, Na, Mg, Al, and Si, as well as for ^{26}Al, are shown in Figures 2 and 3. With the `LUNA` rates, the ^{26}Al abundance decreases by up to 25% and 30% in the $Z = 0.001$ and $Z = 0.0001$ models, respectively, relative to the `JINA` results. For ^{26}Al, we include two data points per model, corresponding to two different mass-loss prescriptions. In particular, in these models, the mass-loss rate is obtained using a mass-loss rate versus period relation [9]. In the first prescription the stellar period is derived using an empirical relation linking the period to the magnitude in the K band [37]. In the second one, the period is computed according to the theoretical non-linear period–mass–radius relation from Trabucchi et al. [38], which was shown to match the observed fundamental-mode period–luminosity sequences in the Magellanic Clouds. Models adopting the first prescription experience fewer third dredge-up (TDU) episodes, shorter lifetimes, and a larger variation in ^{26}Al than those using the second prescription. On the other hand, we get almost no impact in our solar metallicity AGB models at Z = 0.01 and 0.02.

The primary driver of the reduced ^{26}Al production is the lower `LUNA` ^{23}Na(p,γ)^{24}Mg reaction rate. As shown in Figure 1, this is the only reaction in Table 1 that differs significantly from its corresponding `JINA` rate at typical shell H-burning temperatures. In particular, the `LUNA` rate is about an order of magnitude lower than the `JINA` rate at ∼0.07 GK. This reduces the proton capture flow from the NeNa to the MgAl cycle, directly affecting the nucleosynthesis of ^{26}Al. This behavior is also consistent with the larger variations observed for ^{23}Na and ^{24}Mg compared to ^{20}Ne and ^{22}Ne. In models adopting the first mass-loss prescription, the variation in the final ^{26}Al abundance is more pronounced because, with fewer TDU episodes, the surface ^{26}Al is determined mainly by the ^{24}Mg initially present in the envelope. This isotope is progressively converted to ^{25}Mg and locally replenished by p-captures on ^{23}Na in the H–burning shell. In contrast, in models with a reduced mass-loss rate, where many TDU episodes occur, the surface ^{26}Al abundance depends mainly on the ^{25}Mg mixed into the envelope after each TDU; as a result, the differences between the LUNA and `JINA` cases become less pronounced.

This effect is, however, severely limited in our solar metallicity AGB models due to their lower ^{23}Na production compared to the low-metallicity cases. This was already pointed out by [11] and is confirmed by the present work. Indeed, our $Z = 0.01$ model exhibits an approximately constant ^{23}Na abundance in the convective envelope

(which is equivalent to the abundance in the H-burning shell where ^{26}Al is produced); $X(^{23}\mathrm{Na}) = 3 \times 10^{-5}$. By contrast, in our $Z = 0.0001$ model, this value is reached about halfway through the AGB evolution and subsequently increases, peaking at $X(^{23}\mathrm{Na}) = 1 \times 10^{-4}$, i.e., a factor of three higher than in the solar metallicity case.

Furthermore, we note that the higher H-burning temperatures attained in our low-metallicity AGB models may lead to a stronger activation of the MgAl cycle bottleneck reaction ^{24}Mg(p,γ)^{25}Al (the slowest reaction in the (p,γ) chain linking ^{23}Na to ^{26}Al), thereby determining a stronger or weaker impact of the ^{23}Na(p,γ)^{24}Mg reaction on ^{26}Al production. The maximum H-shell burning temperature in our $Z = 0.0001$ model is $T = 6.92 \times 10^7$ K, whereas in our $Z = 0.01$ model, we obtain $T = 6.46 \times 10^7$ K. This temperature difference results in an increase by a factor of ∼12 in the ^{24}Mg(p,γ)^{25}Al nuclear reaction rate.

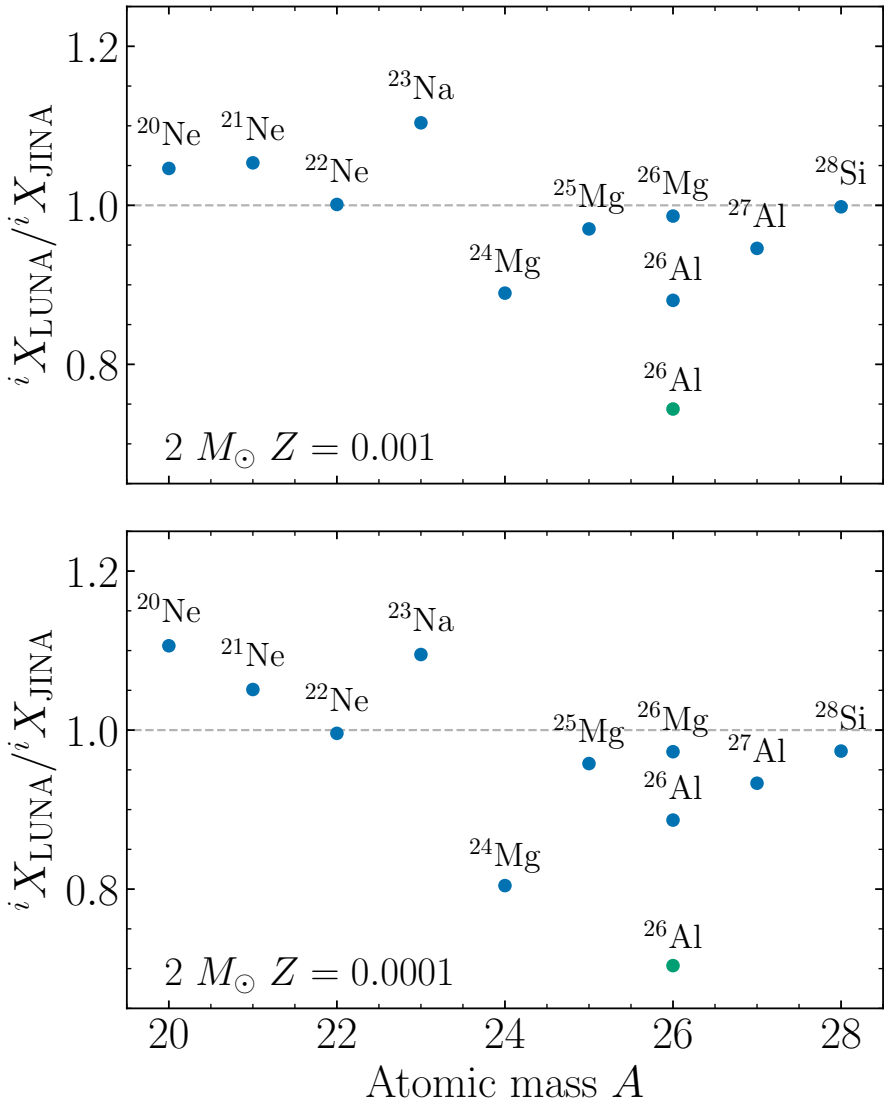

Figure 2. (**Upper panel**): Final surface abundance ratios in our low-mass AGB models at Z = 0.001 of the |LUNA| case relative to the |JINA| case for Ne, Na, Mg, Al and Si stable isotopes and ^{26}Al. The two data points for ^{26}Al show the results obtained adopting two different mass-loss prescriptions (see text for details). (**Lower panel**): same as in the upper panel, but for the Z = 0.0001 case.

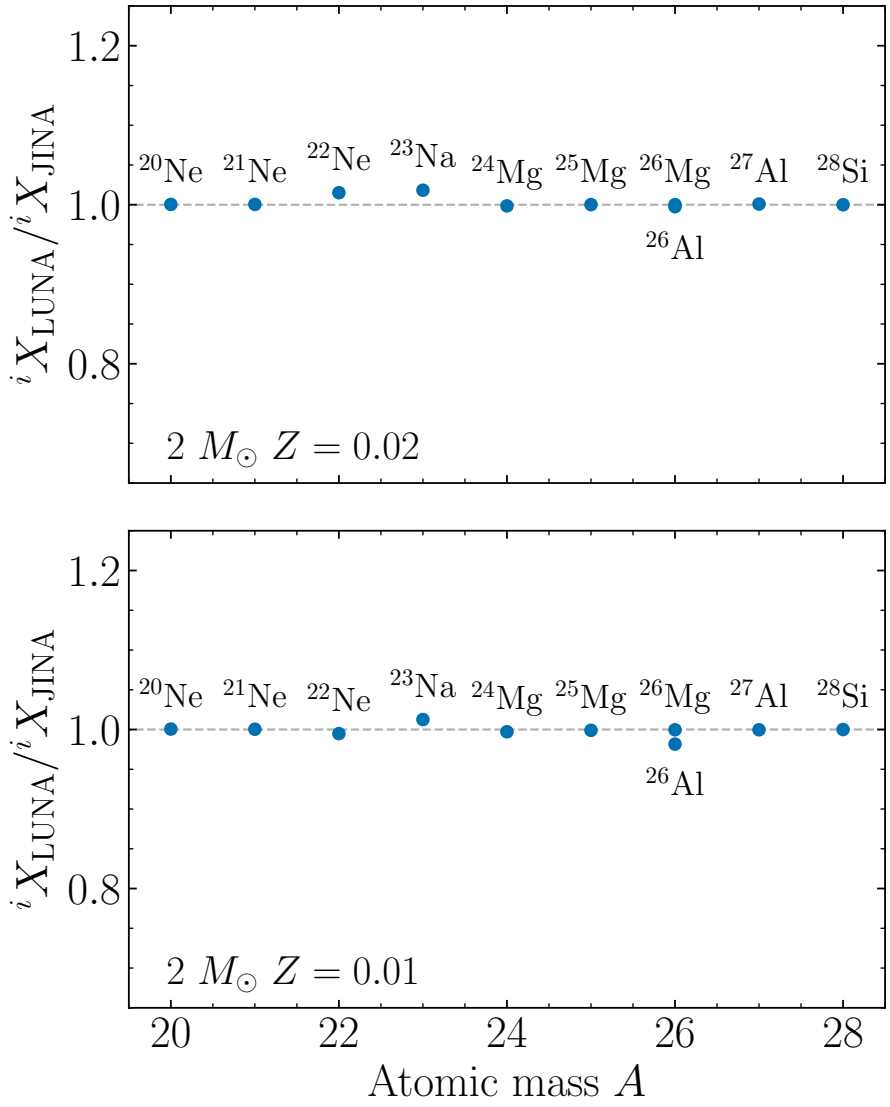

Figure 3. Same as in Figure 2, but for metallicities Z = 0.02 (**Upper panel**) and Z = 0.01 **(Lower panel).**

3.2. Massive Star and Very Massive Star Models

Massive stars are the dominant source of ^{26}Al in the Galaxy through the stellar winds of Wolf–Rayet stars and the ejecta of core-collapse supernovae (CCSNe) (e.g., [39–41]). During hydrostatic convective C-burning, ^{26}Al is efficiently produced via proton capture on abundant ^{25}Mg. The protons are generated directly by C-fusion reactions through the ^{12}C(^{12}C,p)^{23}Na reaction, one of the two main channels driving C-burning (the other being ^{12}C(^{12}C,α)^{20}Ne). At the same time, ^{25}Mg is synthesized primarily through α-particle capture on ^{22}Ne (the α-particles themselves being produced by ^{12}C(^{12}C,α)^{20}Ne) and through neutron capture on ^{24}Mg.

In Figure 4, we present the mass fraction abundance profiles of key nuclear species as a function of the internal mass coordinate in the massive star model discussed in this work. The region shown is the C-burning shell at the end of C-burning, which is both the location and the evolutionary stage at which ^{26}Al production reaches its maximum in our model. The impact of using the `JINA` versus the LUNA reaction rates on ^{26}Al nucleosynthesis is clearly visible. Adopting the LUNA rates when computing shell C-burning nucleosynthesis leads to a ∼51% increase in the ^{26}Al abundance compared to the case using the `JINA` rates.

Both the ^{20}Ne(p,γ)^{21}Na and ^{22}Ne(p,γ)^{23}Na LUNA reaction rates are between ∼15% and ∼20% lower than their JINA counterparts (see Figure 1). ^{20}Ne, one of the main products of C-burning, is about a factor of ∼1000 more abundant than ^{22}Ne in the region where ^{26}Al is produced. At the same time, the ^{22}Ne(p,γ)^{23}Na nuclear reaction rate at the C-burning temperature is in turn about a factor of ∼1000 higher than the ^{20}Ne(p,γ)^{21}Na one. This is why the combined variation in both the ^{20}Ne(p,γ)^{21}Na and ^{22}Ne(p,γ)^{23}Na rate is primarily responsible for the change in ^{26}Al production. The lower LUNA rate results in fewer protons being captured by ^{20}Ne and ^{22}Ne, which in this context effectively behave as proton poisons. Consequently, more protons remain available for capture by ^{25}Mg through the ^{25}Mg(p,γ)^{26}Al reaction, the main production channel of ^{26}Al. Finally, in the lower panel of Figure 4, we also show the impact of the uncertainties affecting the LUNA rates. This impact was not obtained from a full Monte Carlo propagation of the reaction rate uncertainties. Instead, we adopted a conservative "extreme-case" approach to assess the maximum impact of the revised LUNA rates on the surface ^{26}Al abundance. Specifically, we performed a series of dedicated test calculations in which each of the three relevant LUNA reaction rates was individually varied within its quoted uncertainty range, both upward and downward, while keeping the other rates fixed. From these six tests, we identified whether each rate variation led to an increase or a decrease in the resulting ^{26}Al abundance. We then carried out two additional calculations in which all rate variations that maximally increased ^{26}Al were applied simultaneously, and, conversely, all variations that maximally decreased ^{26}Al were combined. The resulting curves therefore bracket the maximum plausible impact of the LUNA nuclear uncertainties on ^{26}Al production and should be regarded as conservative upper and lower limits, rather than statistically defined confidence intervals. Importantly, even these extreme cases remain small compared to the overall difference obtained when adopting the LUNA rates instead of the JINA recommendations. The resulting ^{26}Al variation, while visible, is much smaller ($\leq$10%) compared to the change resulting from the adoption of the LUNA rates vs the JINA ones.

To address the potential impact on VMS, we extended our analysis to a 300 $M_\odot$ solar metallicity stellar model from [42]. This class of objects is particularly relevant, as they may give a large contribution to the galactic ^{26}Al [42]. A large fraction of VMS nucleosynthetic output is released through strong stellar winds during core H-burning and subsequent Wolf–Rayet phases, rather than through a terminal supernova explosion. Indeed, for such high initial masses, direct collapse to a black hole is expected, and no supernova ejecta were considered in this work. In contrast to the 15 $M_\odot$ model discussed above, where the dominant impact of the new LUNA rates on ^{26}Al arises during hydrostatic C-burning at temperatures of $T \sim$ 1–2 GK, more than 90% of the total ejected yields in the 300 $M_\odot$ model are expelled during central H-burning, at significantly lower temperatures of $T \simeq$ (3–6) $\times$ 10^7 K. In this temperature regime, the difference between the JINA and LUNA ^{20}Ne(p,γ)^{21}Na and ^{22}Ne(p,γ)^{23}Na reaction rates drops to below ∼5% and ∼10% respectively, limiting their impact. This results in no measurable variation in the total wind-ejected ^{26}Al yield between the two cases. However, we find a non-negligible effect for specific stable isotopes, most notably ^{21}Ne, whose total ejected yield decreases by ∼13% when adopting the LUNA rates. This behavior is the result of the combination of many factors, including the larger variation in the ^{22}Ne(p,γ)^{23}Na and ^{23}Na(p,γ)^{24}Mg reactions compared to ^{20}Ne(p,γ)^{21}Na at H-burning temperatures. In these conditions, the ^{22}Ne(p,γ)^{23}Na rate exceeds the ^{23}Na(p,γ)^{24}Mg rate by about three orders of magnitude, and the abundance of ^{22}Ne is roughly three times higher than that of ^{23}Na. As a result, the ^{22}Ne(p,γ)^{23}Na reaction dominates the proton capture flow in this region. Since the LUNA rate for ^{22}Ne(p,γ)^{23}Na is ∼10–15% higher than the corresponding JINA rate at these temperatures, it leads to a reduced availability of free protons for capture on ^{20}Ne, the direct production channel of

^{21}Ne, thereby contributing to the observed decrease in its final yield. Table 2 summarizes the total wind-ejected yields of Ne, Na, Mg and Al isotopes for the 300 $M_{\odot}$ model in both the JINA and LUNA cases. The table highlights the selective impact of the new reaction rates on ^{21}Ne, while confirming the absence of any significant effect on ^{26}Al and the other isotopes considered. These results demonstrate that, although VMS dominate the stellar wind contribution to galactic radionuclide budgets, the impact of the new LUNA measurements on ^{26}Al yields is strongly site- and temperature-dependent, and is substantially reduced in environments where nucleosynthesis is governed by low-temperature H-burning.

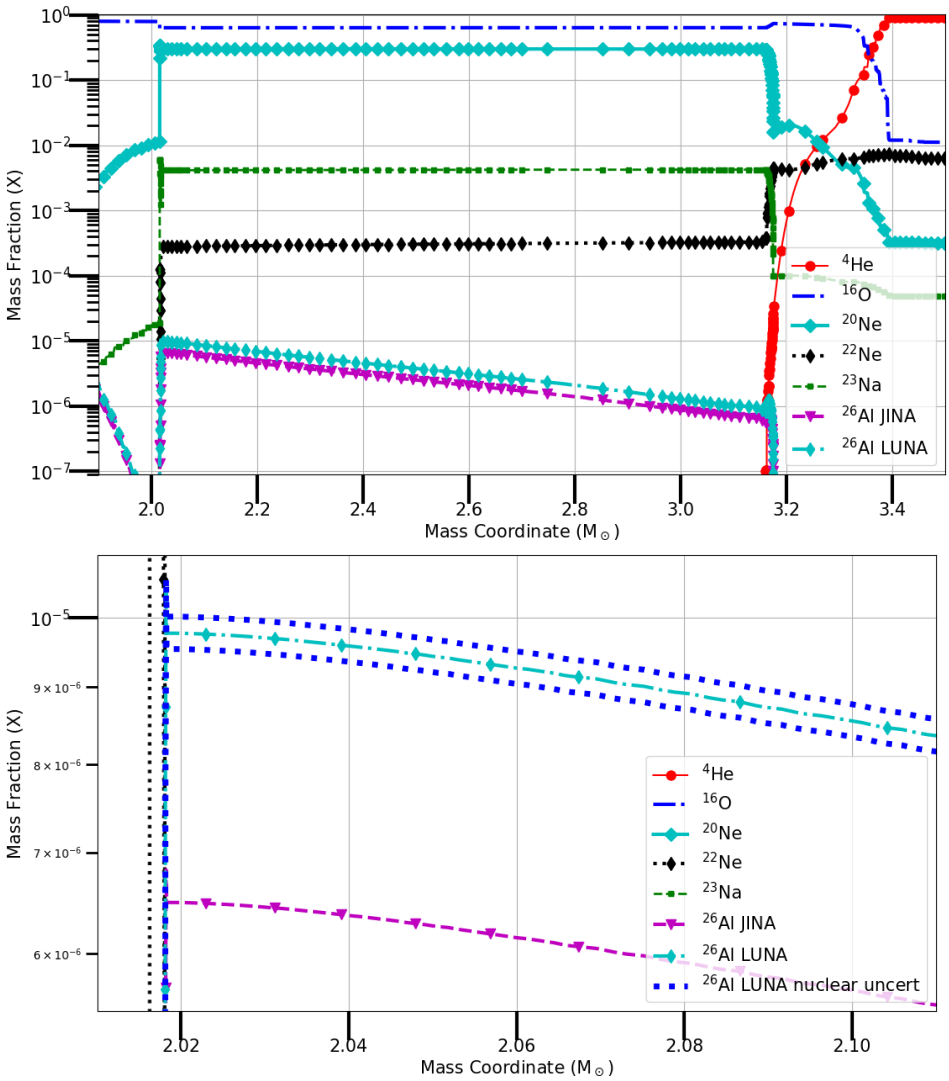

Figure 4. (**Upper panel**): Abundances in mass fraction of key nuclear species as a function of the internal mass coordinate in the massive star model discussed in this work. The stellar region shown is the C-shell at the end of C-burning. The impact of using the JINA rates versus the adoption of LUNA rates on ^{26}Al nucleosynthesis is also presented. (**Lower panel**): Zoomed-in plot of ^{26}Al abundance profiles. The impact of the uncertainties in the nuclear reaction rates discussed in this work is also included.

Table 2. Total wind-ejected yields in solar masses of Ne, Na, Mg and Al isotopes for the 300 $M_\odot$ solar metallicity model from [42], computed using the default JINA reaction rates and the updated LUNA rates.

Element	A	$\text{Yield}_{\text{JINA}}$	$\text{Yield}_{\text{LUNA}}$
Ne	20	5.03×10^{-1}	5.03×10^{-1}
Ne	21	9.16×10^{-4}	7.97×10^{-4}
Ne	22	2.00×10^{-1}	2.00×10^{-1}
Na	23	5.81×10^{-2}	5.85×10^{-2}
Mg	24	1.67×10^{-1}	1.67×10^{-1}
Mg	25	7.23×10^{-3}	7.22×10^{-3}
Mg	26	3.84×10^{-2}	3.82×10^{-2}
Al	26	2.37×10^{-3}	2.37×10^{-3}
Al	27	2.04×10^{-2}	2.06×10^{-2}

3.3. Core-Collapse Supernova Explosions

The explosive single-zone trajectory was extracted from the explosive simulation of a M = 15 $M_\odot$ Z = 0.006 model performed by [12], at a mass coordinate of M = 2.66 $M_\odot$, where the largest production of ^{26}Al is obtained. The local temperature and density peaks during the CCSN explosion are 2.39 GK and 1.18×10^5 g cm^{-3}, respectively.

In Figure 5, the abundance evolution in the CCSN explosive trajectory is shown for two cases, using the JINA rates (thin lines) and LUNA rates (thick lines). Notice how the ^{22}Ne(p, γ)^{23}Na LUNA rate does not cover temperatures up to the peak of our trajectory. We therefore assume that the ∼20% difference at 1 GK compared to the JINA rate is preserved also at higher temperatures, and we simply multiply the JINA rate by 0.8 at all temperatures instead of adopting the actual LUNA rate. The overall ^{26}Al abundance in the mass fraction varies by a negligible amount. This is due to the fact that only the ^{22}Ne(p, γ)^{23}Na reaction presents a non-negligible difference at explosive C-burning nucleosynthesis temperatures between the LUNA and JINA rates. However, as already discussed in Section 3.2, the ^{22}Ne pre-supernova abundance in the C-shell is orders of magnitude lower than other species, such as ^{20}Ne. This, combined with the very short timescales (∼1 s), therefore limits any impact on the overall nucleosynthesis.

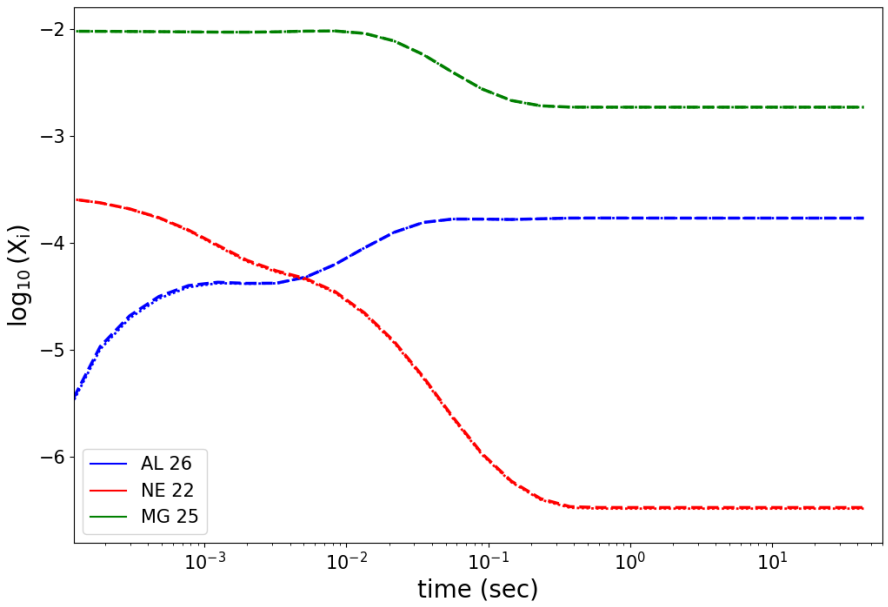

Figure 5. The evolution of the isotopic abundances (mass fractions) of ^{22}Ne, ^{25}Mg, and ^{26}Al is shown during the CCSN explosion using the JINA rates (thin lines) and LUNA rates (thick lines).

4. Conclusions

In this work, we presented a deterministic comparison between default JINA rates and the updated LUNA recommendations (not a full uncertainty propagation via, e.g., a Monte Carlo approach). In particular, we have assessed the impact of the recent LUNA measurements of the ^{20}Ne$(p,\gamma)^{21}$Na, ^{22}Ne$(p,\gamma)^{23}$Na, and ^{23}Na$(p,\gamma)^{24}$Mg reactions on the nucleosynthesis of ^{26}Al in three key astrophysical sites: low-mass AGB stars, hydrostatic C-burning in massive stars, and explosive C-burning in core-collapse supernovae. These measurements, carried out between 2019 and 2024 at the LUNA underground facility, represent the most precise experimental determinations to date of these relevant reaction rates in the NeNa and MgAl cycles. Despite this, they are not yet consistently implemented in commonly used reaction rate libraries, such as JINA REACLIB, motivating the systematic comparison performed in this study.

Our low-mass AGB models show that adopting the LUNA rates leads to a reduction of the final surface abundance of ^{26}Al by up to 25–30%, depending on metallicity and mass-loss prescription. This behavior is driven primarily by the significantly lower LUNA rate for the ^{23}Na$(p,\gamma)^{24}$Mg reaction at typical H-burning shell temperatures, which slows the flow from the NeNa to the MgAl cycle and thereby suppresses ^{26}Al production. The accompanying variations in the abundances of ^{23}Na, ^{24}Mg, and other neighboring isotopes corroborate this interpretation. Additionally, the ^{26}Al left by the H-burning is a neutron poison. Therefore, its reduction/increase may affect the *s*-process distribution produced during the AGB phase.

In the massive star model, by contrast, we find a sizable $\sim$ 51% enhancement of ^{26}Al production in the C-burning shell when using the new LUNA rates. In this case, the dominant contribution arises from the reduced ^{20}Ne(p,γ) and ^{22}Ne(p,γ) rates, which increase the abundance of free protons available for capture on ^{25}Mg, the main hydrostatic production channel of ^{26}Al. We also quantified the impact of the uncertainties affecting the LUNA rates. The resulting ^{26}Al variation, while visible, is much smaller ($\leq$10%) compared to the change resulting from the adoption of the LUNA rates vs the JINA ones. On the other hand, no relevant impact is found in the ejected ^{26}Al yields of our VMS model.

For the explosive nucleosynthesis trajectory extracted from a core-collapse supernova simulation, the impact of the updated rates is negligible. The short timescales of explosive burning, combined with the extremely low pre-explosive abundance of ^{22}Ne in the C-burning shell, effectively limit the influence of the revised NeNa and MgAl reaction flows on ^{26}Al production during the explosion.

Overall, our findings demonstrate that the adoption of the new LUNA reaction rates can lead to significant changes in the predicted nucleosynthesis of ^{26}Al in hydrostatic stellar environments. These differences have direct implications for galactic chemical evolution studies, the inferred galactic budget of ^{26}Al, and theoretical predictions of the ^{60}Fe/^{26}Al ratio, which will be strongly constrained by upcoming γ-ray observations from missions such as COSI .

Concerning the ^{23}Na$(p,\gamma)^{24}$Mg reaction, a few years after the LUNA measurement of the strength of the low-energy 133 keV resonance, Ref. [43] published a revision of the energy for that resonance, based on measurements conducted at the Triangle Universities Nuclear Laboratory (TUNL). In particular, Ref. [43] computed a new reaction rate, consisting of a combination of the resonance strength from the LUNA and their newly measured resonance energy. This resulted in an increased reaction rate by a factor of $\sim$2 at $\sim$0.07 GK. Therefore, it is also very important to consider this TUNL study when deciding which ^{23}Na$(p,\gamma)^{24}$Mg reaction rate to include in the nuclear reaction network before starting any relevant nucleosynthesis study.

https://doi.org/10.3390/universe12030070

Given the astrophysical significance of ^{26}Al, our results highlight the importance of incorporating these updated reaction rates into reaction network libraries used for stellar evolution and nucleosynthesis modeling. Future work should extend this comparison to a broader range of metallicities and stellar masses. Additionally, several nuclear uncertainties affecting ^{26}Al nucleosynthesis still need to be addressed. The LUNA collaboration is currently conducting dedicated experimental campaigns to tackle some of these, such as the ongoing direct measurement and re-evaluation of the $^{24}\mathrm{Mg}(p,\gamma)$, the $^{22}\mathrm{Ne}(\alpha,n)$ and the $^{12}\mathrm{C}+{}^{12}\mathrm{C}$ nuclear reaction rates. Such efforts will be essential to fully quantify the stellar and nuclear physics uncertainties that affect our understanding of the galactic origin of ^{26}Al.

Author Contributions: Conceptualization, U.B.; methodology, U.B.; software, U.B., D.V. and S.C.; validation, U.B. and D.V.; formal analysis, U.B., D.V. and T.G.; investigation, U.B.; resources, U.B., R.H.; data curation, U.B., D.V., E.M. and E.R.H.; writing—original draft preparation, U.B. and D.V.; writing—review and editing, D.V., S.C., A.B., O.S., E.M., R.H. and E.R.H.; visualization, U.B.; supervision, S.C.; project administration, U.B.; funding acquisition, A.B. All authors have read and agreed to the published version of the manuscript.

Funding: This work was supported by the Italian Ministry of Research project FARE 2020, grant R20SLAA8CJ.

Data Availability Statement: The data presented in this study are available upon reasonable request from the authors. The nuclear reaction rates tested in this work are available in a machine-readable format table from both the ChANUREPS nuclear platform (https://chanureps.chetec-infra.eu/, access date 17 February 2026) and the LUNA public reaction rate repository (https://luna.lngs.infn.it/index.php/scientific-output/reaction-rate-repository), access date 17 February 2026.

Acknowledgments: We deeply thank Axel Boeltzig for fruitful discussions that helped improve the present work.

Conflicts of Interest: The authors declare no conflicts of interest.

References

1. Boeltzig, A.; Best, A.; Pantaleo, F.R.; Imbriani, G.; Junker, M.; Aliotta, M.; Balibrea-Correa, J.; Bemmerer, D.; Broggini, C.; Bruno, C.G.; et al. Direct measurements of low-energy resonance strengths of the ^{23}Na(p,γ)^{24}Mg reaction for astrophysics. *Phys. Lett. B* **2019**, *795*, 122–128. [CrossRef]
2. Masha, E.; Barbieri, L.; Skowronski, J.; Aliotta, M.; Ananna, C.; Barile, F.; Bemmerer, D.; Best, A.; Boeltzig, A.; Broggini, C.; et al. First measurement of the low-energy direct capture in ^{20}Ne(p ,γ)^{21}Na and improved energy and strength of the $E_{c.m.}$=368 keV resonance. *Phys. Rev. C.* **2023**, *108*, L052801. [CrossRef]
3. Takács, M.P.; Ferraro, F.; Piatti, D.; Skowronski, J.; Aliotta, M.; Ananna, C.; Barbieri, L.; Barile, F.; Bemmerer, D.; Best, A.; et al. Direct capture cross section and resonances in the ^{22}Ne(p ,γ)^{23}Na reaction at low energy. *Phys. Rev. C.* **2024**, *109*, 064627. [CrossRef]
4. Battino, U.; Roberti, L.; Lawson, T.V.; Laird, A.M.; Todd, L. Impact of Newly Measured Nuclear Reaction Rates on ^{26}Al Ejected Yields from Massive Stars. *Universe* **2024**, *10*, 204. [CrossRef]
5. Laird, A.M.; Lugaro, M.; Kankainen, A.; Adsley, P.; Bardayan, D.W.; Brinkman, H.E.; Côté, B.; Deibel, C.M.; Diehl, R.; Hammache, F.; et al. Progress on nuclear reaction rates affecting the stellar production of ^{26}Al. *J. Phys. G Nucl. Phys.* **2023**, *50*, 033002. [CrossRef]
6. Diehl, R.; Halloin, H.; Kretschmer, K.; Lichti, G.G.; Schönfelder, V.; Strong, A.W.; von Kienlin, A.; Wang, W.; Jean, P.; Knödlseder, J.; et al. Radioactive ^{26}Al from massive stars in the Galaxy. *Nature* **2006**, *439*, 45–47. [CrossRef]
7. Tomsick, J.; Zoglauer, A.; Sleator, C.; Lazar, H.; Beechert, J.; Boggs, S.; Roberts, J.; Siegert, T.; Lowell, A.; Wulf, E.; et al. The Compton Spectrometer and Imager. *arXiv* **2023**. [CrossRef]
8. Paxton, B.; Bildsten, L.; Dotter, A.; Herwig, F.; Lesaffre, P.; Timmes, F. Modules for Experiments in Stellar Astrophysics (MESA). *Astrophys. J. Suppl. Ser.* **2011**, *192*, 3. [CrossRef]
9. Straniero, O.; Gallino, R.; Cristallo, S. s process in low-mass asymptotic giant branch stars. *Nucl. Phys. A* **2006**, *777*, 311–339. [CrossRef]

10. Cristallo, S.; Straniero, O.; Gallino, R.; Piersanti, L.; Domínguez, I.; Lederer, M.T. Evolution, Nucleosynthesis, and Yields of Low-Mass Asymptotic Giant Branch Stars at Different Metallicities. *Astrophys. J. Suppl. Ser.* **2009**, *696*, 797–820. [CrossRef]
11. Cristallo, S.; Gallino, R.; Straniero, O.; Piersanti, L.; Domınguez, I. Short-lived isotopes and ^{23}Na production in low mass AGB Stars. *arXiv* **2006**. [CrossRef]
12. Ritter, C.; Herwig, F.; Jones, S.; Pignatari, M.; Fryer, C.; Hirschi, R. NuGrid stellar data set-II. Stellar yields from H to Bi for stellar models with M_{ZAMS} = 1–25 $M_{\odot}$ and Z = 0.0001–0.02. *Mon. Not. R. Astron. Soc.* **2018**, *480*, 538–571. [CrossRef]
13. Pignatari, M.; Herwig, F.; Hirschi, R.; Bennett, M.; Rockefeller, G.; Fryer, C.; Timmes, F.X.; Ritter, C.; Heger, A.; Jones, S.; et al. NuGrid Stellar Data Set. I.Stellar Yields from H to Bi for Stars with Metallicities Z = 0.02 and Z = 0.01. *Astrophys. J. Suppl. Ser.* **2016**, *225*, 24. [CrossRef]
14. Wiescher, M.; deBoer, R.J.; Görres, J. The resonances in the ^{22}Ne+α fusion reactions . *Eur. Phys. J. A* **2023**, *59*, 11. [CrossRef]
15. Dietz, M.; Lederer-Woods, C.; Tattersall, A.; Battino, U.; Gunsing, F.; Heinitz, S.; Krtička, M.; Lerendegui-Marco, J.; Reifarth, R.; Valenta, S.; et al. Measurement of the ^{72}Ge (n ,γ) cross section over a wide neutron energy range at the CERN n_TOF facility. *Phys. Rev. C.* **2021**, *103*, 045809. [CrossRef]
16. Gawlik-Ramiega, A.; Lederer-Woods, C.; Krtička, M.; Valenta, S.; Battino, U.; Andrzejewski, J.; Perkowski, J.; Aberle, O.; Audouin, L.; Bacak, M.; et al. Measurement of the ^{76}Ge(n ,γ) cross section at the n_TOF facility at CERN. *Phys. Rev. C.* **2021**, *104*, 044610. [CrossRef]
17. Sosnin, N. V.; Lederer-Woods, C.; Krtička, M.; Garg, R.; Dietz, M.; Bacak, M.; Barbagallo, M.; Battino, U.; Cristallo, S.; Damone, L.A.; et al. Measurement of the ^{77}Se(n ,γ) cross section up to 200 keV at the n_TOF facility at CERN. *Phys. Rev. C.* **2023**, *107*, 065805. [CrossRef]
18. Sosnin, N. V.; Lederer-Woods, C.; Garg, R.; Battino, U.; Cristallo, S.; Dietz, M.; Heinitz, S.; Krtička, M.; Reifarth, R.; Valenta, S.; et al. Measurement of the ^{78}Se(n,γ)^{79}Se cross section up to 600 keV at the n_TOF facility at CERN. *Phys. Rev. C.* **2024**, *110*, 065805. [CrossRef]
19. Battino, U.; Lederer-Woods, C.; Pignatari, M.; Soós, B.; Lugaro, M.; Vescovi, D.; Cristallo, S.; Woods, P.J.; Karakas, A. Impact of newly measured ^{26}Al(n, p)^{26}Mg and ^{26}Al(n, α)^{23}Na reaction rates on the nucleosynthesis of ^{26}Al in stars. *Mon. Not. R. Astron. Soc.* **2023**, *520*, 2436–2444. [CrossRef]
20. Vescovi, D.; Cristallo, S.; Busso, M.; Liu, N. Magnetic-buoyancy-induced Mixing in AGB Stars: Presolar SiC Grains. *Astrophys. J. Lett.* **2020**, *897*, L25. [CrossRef]
21. Vescovi, D.; Cristallo, S.; Palmerini, S.; Abia, C.; Busso, M. Magnetic-buoyancy-induced mixing in AGB stars: Fluorine nucleosynthesis at different metallicities. *Astron. Astrophys.* **2021**, *652*, A100. [CrossRef]
22. Magrini, L.; Vescovi, D.; Casali, G.; Cristallo, S.; Viscasillas Vázquez, C.; Cescutti, G.; Spina, L.; Van Der Swaelmen, M.; Randich, S. Magnetic-buoyancy-induced mixing in AGB stars: A theoretical explanation of the non-universal relation of [Y/Mg] to age. *Astron. Astrophys.* **2021**, *646*, L2. [CrossRef]
23. Liu, N.; Stephan, T.; Cristallo, S.; Vescovi, D.; Gallino, R.; Nittler, L.R.; Alexander, C.M.O.; Davis, A.M. Presolar silicon carbide grains of types Y and Z: Their strontium and barium isotopic compositions and stellar origins. *Eur. Phys. J. A* **2022**, *58*, 216. [CrossRef]
24. Vescovi, D. Mixing and Magnetic Fields in Asymptotic Giant Branch Stars in the Framework of FRUITY Models. *Universe* **2021**, *8*, 16. [CrossRef]
25. Lodders, K. Relative Atomic Solar System Abundances, Mass Fractions, and Atomic Masses of the Elements and Their Isotopes, Composition of the Solar Photosphere, and Compositions of the Major Chondritic Meteorite Groups. *Space Sci. Rev.* **2021**, *217*, 44. [CrossRef]
26. Magg, E.; Bergemann, M.; Serenelli, A.; Bautista, M.; Plez, B.; Heiter, U.; Gerber, J.M.; Ludwig, H.G.; Basu, S.; Ferguson, J.W.; et al. Observational constraints on the origin of the elements. IV. Standard composition of the Sun. *Astron. Astrophys.* **2022**, *661*, A140. [CrossRef]
27. Ciani, G.F.; Csedreki, L.; Rapagnani, D.; Aliotta, M.; Balibrea-Correa, J.; Barile, F.; Bemmerer, D.; Best, A.; Boeltzig, A.; Broggini, C.; et al. Direct Measurement of the C 13 (α ,n)O 16 Cross Section into the *s*-Process Gamow Peak. *Phys. Rev. Lett.* **2021**, *127*, 152701. [CrossRef]
28. Cyburt, R.H.; Amthor, A.M.; Ferguson, R.; Meisel, Z.; Smith, K.; Warren, S.; Heger, A.; Hoffman, R.D.; Rauscher, T.; Sakharuk, A.; et al. The JINA REACLIB Database: Its Recent Updates and Impact on Type-I X-ray Bursts. *Astrophys. J. Suppl. Ser.* **2010**, *189*, 240–252. [CrossRef]
29. Lyons, S.; Görres, J.; deBoer, R.J.; Stech, E.; Chen, Y.; Gilardy, G.; Liu, Q.; Long, A.M.; Moran, M.; Robertson, D.; et al. Determination of ^{20}Ne(p ,γ)^{21}Na cross sections from E_p=500–2000 keV. *Phys. Rev. C.* **2018**, *97*, 065802. [CrossRef]
30. Kelly, K.J.; Champagne, A.E.; Downen, L.N.; Dermigny, J.R.; Hunt, S.; Iliadis, C.; Cooper, A.L. New measurements of low-energy resonances in the ^{22}Ne(p ,γ)^{23}Na reaction. *Phys. Rev. C.* **2017**, *95*, 015806. [CrossRef]
31. Iliadis, C.; Longland, R.; Champagne, A.E.; Coc, A.; Fitzgerald, R. Charged-particle thermonuclear reaction rates: II. Tables and graphs of reaction rates and probability density functions. *Nucl. Phys. A* **2010**, *841*, 31–250. [CrossRef]

32. Straniero, O.; Imbriani, G.; Strieder, F.; Bemmerer, D.; Broggini, C.; Caciolli, A.; Corvisiero, P.; Costantini, H.; Cristallo, S.; DiLeva, A.; et al. Impact of a Revised ^{25}Mg(p, γ)^{26}Al Reaction Rate on the Operation of the Mg-Al Cycle. *Astrophys. J.* **2013**, *763*, 100. [CrossRef]
33. Forestini, M.; Arnould, M.; Paulus, G. On the production of Al-26 in AGB stars. *Astron. Astrophys.* **1991**, *252*, 597–604.
34. Iben, I., Jr. Thermal pulses: *p*-capture, α-capture, *s*-process nucleosynthesis; and convective mixing in a star of intermediate mass. *Astrophys. J.* **1975**, *196*, 525–547. [CrossRef]
35. Straniero, O.; Gallino, R.; Busso, M.; Chiefei, A.; Raiteri, C.M.; Limongi, M.; Salaris, M. Radiative ^{13}C Burning in Asymptotic Giant Branch Stars and *s*-Processing. *Astrophys. J. Part 2-Lett.* **1995**, *440*, L85–L87. [CrossRef]
36. Herwig, F. Evolution of Asymptotic Giant Branch Stars. *Annu. Rev. Astron. Astrophys.* **2005**, *43*, 435–479. [CrossRef]
37. Abia, C.; de Laverny, P.; Cristallo, S.; Kordopatis, G.; Straniero, O. Properties of carbon stars in the solar neighbourhood based on Gaia DR2 astrometry. *Astron. Astrophys.* **2020**, *633*, A135. [CrossRef]
38. Trabucchi, M.; Mowlavi, N.; Lebzelter, T. Semi-regular red giants as distance indicators. I. The period-luminosity relations of semi-regular variables revisited. *Astron. Astrophys.* **2021**, *656*, A66. [CrossRef]
39. Timmes, F.X.; Woosley, S.E.; Weaver, T.A. Galacti chemical evolution: Hygrogen through zinc. *Astrophys. J. Suppl. Ser.* **1995**, *98*, 617–658. [CrossRef]
40. Limongi, M.; Chieffi, A. The Nucleosynthesis of ^{26}Al and ^{60}Fe in Solar Metallicity Stars Extending in Mass from 11 to 120 M_{solar}: The Hydrostatic and Explosive Contributions. *Astrophys. J.* **2006**, *647*, 483–500. [CrossRef]
41. Lawson, T.V.; Pignatari, M.; Stancliffe, R.J.; den Hartogh, J.; Jones, S.; Fryer, C.L.; Gibson, B.K.; Lugaro, M. Radioactive nuclei in the early Solar system: Analysis of the 15 isotopes produced by core-collapse supernovae. *Mon. Not. R. Astron. Soc.* **2022**, *511*, 886–902. [CrossRef]
42. Higgins, E.R.; Vink, J.S.; Hirschi, R.; Laird, A.M.; Sabhahit, G.N. Stellar wind yields of very massive stars. *Mon. Not. R. Astron. Soc.* **2023**, *526*, 534–547. [CrossRef]
43. Marshall, C.; Setoodehnia, K.; Portillo, F.; Kelley, J.H.; Longland, R. New energy for the 133-keV resonance in the ^{23}Na(p,γ)^{24}Mg reaction and its impact on nucleosynthesis in globular clusters. *Phys. Rev. C* **2021**, *104*, L032801. [CrossRef]